WIRELESS COMMUNICATIONS AND MOBILE COMPUTING
Wirel. Commun. Mob. Comput. **10**: 609–621 (2010)
Published online in Wiley InterScience
(www.interscience.wiley.com) DOI: 10.1002/wcm.736

Simulation study of IEEE 802.15.4 LR-WPAN for industrial applications

Feng Chen[1,2]*, Nan Wang[2], Reinhard German[2] and Falko Dressler[2]

[1]*Siemens AG, Automation and Drives, Germany*
[2]*Computer Networks and Communication Systems, Department of Computer Science, University of Erlangen-Nuremberg, Martensstr. 3, 91058 Erlangen, Germany*

Summary

The IEEE 802.15.4 protocol has become the primary solution for many Low-Rate Wireless Personal Area Network (LR-WPAN) applications. This is especially the case for industrial sensor network applications such as automation control. We contribute to the better understanding of the protocol behavior by presenting a set of results of simulation experiments. Our results outline the capabilities of this protocol in the selected scenarios but also the limitations. In particular, we investigated the dependency of the protocol on protocol-inherent parameters such as the beacon order and the superframe order but also to different traffic load. Our results can be used for planning and deploying IEEE 802.15.4 based sensor networks with specific performance demands. We put a special focus on application scenarios in industrial sensor network applications. The primary requirements are reduced end-to-end latency and energy consumption. Our studies are based on our new implementation of IEEE 802.15.4 developed for the simulation framework OMNeT++. Copyright © 2010 John Wiley & Sons, Ltd.

KEY WORDS: IEEE 802.15.4 LR-WPAN; performance evaluation; simulation

1. Introduction

The IEEE 802.15.4 [7] protocol is an industrial standard for Low-Rate Wireless Personal Area Network (LR-WPAN) architectures. As the primary application domain Wireless Sensor Network (WSN) applications in industrial environments can be identified. For example, the department "Automation and Drives, A&D" of Siemens AG is currently evaluating wireless technology in the field of industrial automation. Thus, LR-WPAN is intended to become an enabling technology for WSNs [1, 2]. In contrast to Wireless Local Area Network (WLAN), which is standardized by IEEE 802.11 family, LR-WPAN stresses short-range operation, low-data-rate, energy-efficiency, and low-cost. An example is ZigBee [18], which is an open specification built on the LR-WPAN standard and focusing on the establishment and maintenance of LR-WPANs. Such networks are designed for low-rate applications, however they especially stress energy efficiency.

IEEE 802.15.4 defines the specifications of the Physical Layer (PHY) and Medium Access Control (MAC) sublayer. Products that implement this standard are commercially available at an acceptable low cost. One of the first investigations of the applicability of IEEE 802.15.4 in industrial applications has been performed by Bougard et al. [3], whereas the

*Correspondence to: Computer Networks and Communication Systems, Department of Computer Science, University of Erlangen-Nuremberg, Martensstr. 3, 91058 Erlangen, Germany. E-mail: feng.chen@informatik.uni-erlangen.de

authors concentrated on dense deployment scenarios as studied in the WSN community. Zheng et al. developed a simulation model of LR-WPAN for The Network Simulator 2 (ns-2), based on which they presented a comprehensive performance study of IEEE 802.15.4 [17]. However, the ns-2 model was built complying with an earlier standard edition (IEEE 802.15.4 draft D18), which has been nowadays replaced by the latest revised release IEEE Std 802.15.4-2006. Moreover, the GTS mechanism was not implemented in the ns-2 model. In the framework of open-ZB project [6] that aims to provide open source toolset for IEEE 802.15.4 and ZigBee, an OPNET simulation model for the IEEE 802.15.4 beacon-enabled mode supporting the star topology has been built to evaluate the performance of the slotted CSMA/CA mechanism [11]. As an extension to the previous work, an OPNET model for the IEEE 802.15.4 GTS mechanism was developed by Jurcik et al. in [8], based on which the performance of the GTS mechanism was investigated in terms of throughput and delay. However, energy performance has not been considered in previously described work that relies on the developed OPNET model.

In this paper, we study the applicability of the LR-WPAN techniques in industrial control applications. This application scenario is of special interest because sensor network technology is increasingly demanded in this domain and the IEEE standard provides a protocol developed and accepted in the industry compared to other solutions such as S-MAC [16]. We develop a simulation model of the current protocol version of IEEE 802.15.4 using OMNeT++, which is an open-architecture network simulator. Through extensive simulations based on our model, we analyze the IEEE 802.15.4 protocol in a parameter range and environment as typically required in industrial automation scenarios. We expect that a number of sensor nodes are scattered within an area and associated to a central node to form a star network, which is continuously monitoring industrial processes. Once a certain device detects that particular sensor readings exceed a predefined threshold, a short alarm message must be sent by the device to the central node within a given time frame. These parameters have been chosen to match the peculiarities in specific industrial automation scenarios that for example Siemens A&D is working on. We discusses the requirements with industrial partners and it turned out that energy-efficient single-hop communication in a star network with specific latency demands is representing the current needs in automation facilities.

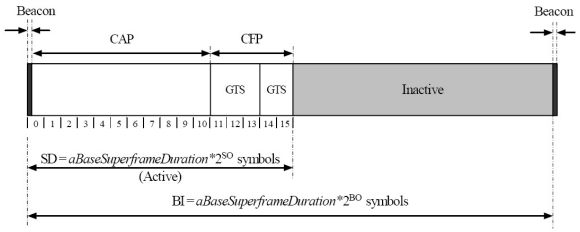

Fig. 1. IEEE 802.15.4 superframe structure

The remainder of the paper is organized as follows. Section 2 gives a brief description of IEEE 802.15.4 protocols. In Section 3, we introduce an IEEE 802.15.4 model in OMNeT++, as well as its settings and configurations for our simulation study. In Section 4, our simulation results from various scenarios are presented and explained. Finally, Section 5 concludes the paper and gives a vision to the future work.

2. Overview of IEEE 802.15.4

In this section, a brief overview to the IEEE 802.15.4 protocol is provided. For a more detailed description of the protocol, the reader is recommended to refer to the protocol standard documents [7] and to [2].

The IEEE 802.15.4 Wireless Personal Area Network (WPAN) can operate in one of three ISM frequency bands and choose from a total of 27 channels. Two different types of devices are defined in an LR-WPAN: a full function device (FFD) and a reduced function device (RFD). A FFD can talk to any other device and serves as a PAN coordinator, a coordinator, or a device. An RFD can only talk to an FFD node. Furthermore, the standard supports two network topologies, a star and a peer-to-peer topology. In star networks, the communication occurs only between end devices and a single central controller, which is called the PAN coordinator and which manages the entire PAN. In peer-to-peer topology, a PAN coordinator is used also. However, it differs from the star topology as any of the devices can arbitrarily communicate with each other as long as they are within a common wireless communication range. A special case of the peer-to-peer topology is the cluster tree. In this case, a node may only talk to its parent or children nodes.

In order to synchronize the communication at MAC layer, the IEEE 802.15.4 PAN can optionally operate in the so called *beacon-enabled* mode. In this case, a superframe structure is used as shown in

DOI: 10.1002/wcm

Figure 1. Each *superframe* is bounded by periodically transmitted beacon frames, which allow nodes to associate with and synchronize to their coordinator. Each superframe consists of two parts, an active portion and an inactive portion. In order to save energy, nodes may enter a low-power (sleep) mode during the inactive portion. The superframe structure is specified by the values of two MAC attributes: the *macBeaconOrder* (BO) and the *macSuperframeOrder* (SO). Both of which determine the length of the beacon interval (BI) and the length of the active portion of the superframe (SD), respectively. The relation of BO to BI and the relation of SO to SD are shown in Figure 1. The *aBaseSuperframeDuration* equals to 960 symbols. PANs that wish to use this superframe structure (referred to as a beacon-enabled PANs), shall set BO to a value between 0 and 14 and SO to a value between 0 and the value of BO, resulting in the range of BI and SD between $15.36\,\mathrm{ms}$ and $251.7\,\mathrm{s}$ at the $2.4\,\mathrm{GHz}$ band. If BO=15, PANs operate in a so-called *nonbeacon-enabled* mode without using the superframe structure.

The active portion of the superframe shall be divided into 16 equally spaced slots, which are called *superframe slots*. The duration of one superframe slot is calculated by $2^{SO} \times aBaseSlotDuration$, where the default value of *aBaseSlotDuration* is 60 symbols. There are three parts in the active portion: a beacon, a Contention Access Period (CAP), and a Contention-Free Period (CFP). In the CAP, all data transmissions shall follow a successful execution of a slotted CSMA-CA algorithm. Two data transfer models are defined in the CAP, the indirect transmission for downlink data and the direct transmission for uplink data.

For application scenarios requiring low-latency or specific data rates, the PAN coordinator may dedicate portions of the active superframe to that application, which are called guaranteed time slots (GTSs). They allow the channel access in TDMA-like fashion. The GTSs form the Contention-Free Period, which starts on a slot boundary immediately following the CAP and ends before the beginning of the inactive portion, as shown in Figure 1. The PAN coordinator may allocate a maximum of seven GTSs at the same time, and one GTS may occupy more than one superframe slot. The allocated GTSs shall be located within the CFP and occupy contiguous slots. Therefore, the CFP shall grow or shrink dynamically within the active portion depending on the total length of all of the current existing GTSs. However, a minimum length of the CAP with *aMinCAPLength* (440) symbols must be guaranteed and remains for contention-based access of other networked devices or new devices wishing to join the network. An exception to this minimum shall be allowed for the accommodation of the temporary increase in the beacon frame length needed to perform GTS maintenance as described in [7].

3. Simulation Setup

In this paper we utilize simulation techniques to evaluate the performance of the IEEE 802.15.4 protocols. The evaluation is performed using a simulation model of IEEE 802.15.4 that we developed in OMNeT++ [15]. In this section, we introduce this model and describe the simulation settings.

3.1. IEEE 802.15.4 Model in OMNeT++

We first present a simulation model of IEEE 802.15.4 in OMNeT++/INET framework. OMNeT++ is a public-source, component-based and discrete event simulation environment and has become increasingly popular especially in communications and networking community. Its primary application area covers the simulation of communication networks. Nevertheless, other types of event based simulation are addressed as well including systems and business processes. We also used the INET framework, which is an open-source communication networks simulation package for OMNeT++ and suited for simulations of different kinds of wired and wireless networks. A great number of protocols are already available in this framework.

In contrast to the existing two simulation models in ns-2 and OPNET as described in Section 1, our IEEE 802.15.4 model in OMNeT++ has been built conforming to the latest version of the standard IEEE 802.15.4-2006 in an open-architecture simulation environment. As shown in Figure 2, the model consists of an IEEE 802.15.4 based protocol stack and two protocol-independent modules supporting energy measurement and mobility in the simulations. A screen snapshot of the model in the graphical interface of OMNeT++ is shown in Figure 3. In the following, we briefly introduce the functionality of each module. Further information about the model can be found in [4, 5].

IEEE 802.15.4 MAC and PHY modules – These two modules are the core of the implementation and modeled strictly conforming to the IEEE standard 802.15.4-2006. The PHY module implements the following functions.

DOI: 10.1002/wcm

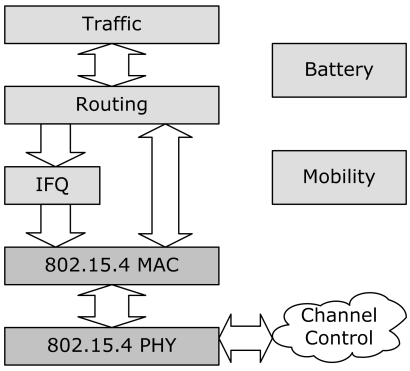

Fig. 2. The structure and components of the LR-WPAN model in OMNeT++

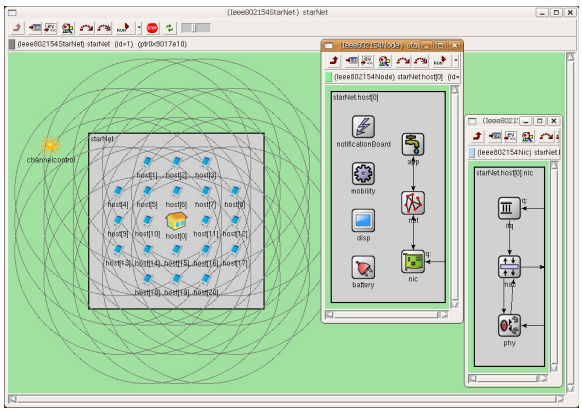

Fig. 3. The screen snapshot of the LR-WPAN model in the graphical user interface of OMNeT++

- Radio implemented in both a three-switch-state model (*receiver-on, transmitter-on, turnoff*) facilitating implementation of MAC-PHY primitives and a four-work-state model (*idle, sleep, receiving, and transmitting*) for the purpose of energy measurement and carrier sensing
- Packets transmission/reception with collision detection
- Energy detection (ED) and clear channel access (CCA)
- Ideal/lossy channel supporting channel switch

In the MAC module, we have concentrated on modeling the data transfer related functions, including the following functions.

- Both slotted and unslotted CSMA-CA
- Both beaconed and non-beaconed mode
- Direct, indirect, and GTS data transfer models
- Interframe spacing (IFS), frame filtering and duplication detection
- Association with coordinators

As for PAN formation and management functions defined in the MAC specification, only a simplified association process has been implemented. In addition, security related specifications [14] are not yet considered in our model.

IFQ module – Because no information about the MAC buffer size is explicitly specified in the standard, we added an interface queue (IFQ) module that acts as the buffer of the MAC layer. The IFQ module represents a drop-tail FIFO queue, which buffers data packets coming from the upper layer and feeds them to the MAC upon request. The buffer size is adjustable.

Routing module – The routing module supports packet forwarding in star and cluster-tree topologies as well as to support the formation of cluster-tree PANs. In this paper, however, the routing module plays no role, because only single-hop communication is considered.

Traffic module – It plays the role of a packet generator at all source nodes or the role of a packet collector consuming these packets at sink nodes. Using a flexible XML-based parameter structure, it can be configured to generate various types of traffic, including the usual constant bit rate (CBR), on-off, and exponentially distributed traffic.

Battery and mobility modules – The battery module provides real-time measurement of energy consumption at each node and supports simulations of network lifetime. By tracking the current radio state in the PHY module, the battery module counts the total time that the radio has spent in each of the four working states and calculates the corresponding energy consumption using the given radio power values. Our battery model provides real-time calculation of energy consumption and can display the remaining energy level for each node in the animation. In addition, it can easily be adapted for evaluation of the network lifetime as a primary result of our simulations. Our model currently relies on energy measurements for the CC1000 radio on Mica2 motes [13]. Nevertheless, it can easily be updated to any other hardware, e.g. the CC2420 radio specially designed for IEEE 802.15.4, if exact measurements are provided.

The mobility module supports simulating static or dynamic topologies. For static simulations, nodes can

be placed at a fixed position or be spread randomly within a specified area. The random placement is useful in simulations that evaluate the formation of cluster-tree networks for application in sensor networks.

3.2. Simulation Settings

We describe now the configuration and settings of the IEEE 802.15.4 model in OMNeT++ for our performance study, including model configurations, parameter settings and definition of performance measures.

As mentioned in the previous section, star networks have advantages compared to mesh networks in terms of robustness and latency. These two aspects are often put into first consideration in many industrial control applications. Sensor networks are still being evaluated for applications in automation processes. IEEE 802.15.4 is a perfect candidate for these environment due to various reasons including the available industry standard. Objectives are usually a high reliability of the communication, energy efficiency, and low latency.

Therefore, we focus in this paper on IEEE 802.15.4 based star networks. Energy consumption is one of the most important considerations in choosing or designing sensor networks for industrial applications. The beaconing synchronization mechanism in IEEE 802.15.4 enables networks to work under a controllable duty cycle to achieve better energy efficiency compared to the non-beacon mode. Therefore, the beacon-enabled mode has been chosen in all our simulations. In Table I, some important model parameters fixed throughout our study are listed. Other internal protocol parameters use default values specified in the IEEE standard. Variable parameters together with scenarios and corresponding results will be introduced in the next section.

The performance of IEEE 802.15.4 based star networks for industrial applications is evaluated in terms of two aspects, energy performance and end-to-end communication performance. One energy measure and three end-to-end measures have been used as described in the following:

- *Energy consumption per payload byte* – the average energy consumed for successfully transmitting one payload byte from the source to the sink by the whole network
- *End-to-end packet loss rate (PLR)* – the ratio of the number of packets dropped by the network (both at IFQ due to queue overflow and at MAC due to exceeding maximum retries) to the total number of packets generated at the source nodes
- *End-to-end delay* – the average delay for a single packet from source to sink
- *End-to-end goodput* – the average number of payload bytes received at the sink node per time unit

Table I. Fixed Model Parameters

PHY Module Parameters	
Channel number, bitrate	11, 250 kb/s
Transmitter power	1 mW
Transmission range	172 m
Carrier sense sensitivity	-85 dBm
MAC and IFQ Module Parameters	
Synchronization mode	beacon-enabled
Topology type	star
IFQ size (buffer)	1
Traffic Module Parameters	
Traffic type	exponential
Payload size	1 Byte
Battery Module Parameters	
Radio power in sleeping	0.06 mA
Radio power in idle	1.38 mA
Radio power in receiving	9.6 mA
Radio power in sending	17 mA

In all our experiments, statistical significance of the simulation results has been carefully considered. For every simulation with the same input parameters, we run five independent replications, from which the mean value is calculated for each performance measure and plotted as a single point in the graph. The simulation time required for each simulation varies drastically with the input traffic and parameter settings, however, it has been chosen long enough to guarantee that more than 5000 packets are received by the sink at the end of each running. The simulation results were plotted in the form of linespoints without errorbar, because the maximum relative standard deviation of the results is less than 1%, which could be unobservable on the graphs.

4. Simulation Results

The previous section described the common settings for our simulations. In this section, the simulation results for IEEE 802.15.4 contention-based and contention free media access mechanisms are presented and discussed.

4.1. First Experiment: IEEE 802.15.4 CSMA/CA

In the first experiment, we evaluate the contention-based media assessment of IEEE 802.15.4 in two selected scenarios. In particular, we analyzed a 3 node scenario and a 21 node scenario as described in the following.

4.1.1. Scenario 1: 3 nodes, 50% Duty Cycle

In the first scenario, we studied a star network with one PAN coordinator and two devices. These three nodes are placed in a row, with the PAN coordinator located in the middle of the other two nodes. To introduce the hidden terminal problem, the distance between the two outer devices is 200 meters, which exceeds the preset radio transmission range of 172 meters as listed in Table I. One device is attached with an exponential traffic source and sends packets via the PAN coordinator to the other device. The duty cycle is set to 50% in all the nodes, however, configured with various combination of BO and SO.

For schedule-based MAC protocols such as IEEE 802.15.4, which defines a superframe structure with periodic active and sleeping periods, it is assumed that the duty cycle should determine the level of the overall energy consumption. We intended to validate this assumption in our simulations. In addition, we were also interested to see how the end-to-end performance of the studied network will be affected by various parameter configurations (mainly BO and SO) and traffic conditions with constant duty cycle. The simulation results are plotted on graphs for each performance measure. Due to a wide variation range in the measured values, logarithmic scaling has been applied on the vertical axis on all the graphs for this scenario exclusive of that for PLR.

Figure 4(a) shows the measured mean energy consumption for transmitting one Byte payload plotted on a logarithmic scale. As expected beforehand, under the same duty cycle, energy consumption shows to be less sensitive to the parameter combination than to the traffic load. For the same (BO,SO), the energy consumption decreases with increasing traffic load, because the average number of transmitted packets per beacon interval increases rapidly – this can be also observed in the goodput graph as shown in Figure 4(d). However, the energy consumption per beacon interval does not increase as significantly as the number of sent packets does, because the increased energy consumed for transmitting more packets does not increase the overall energy consumption per beacon too much in the case of the same duty cycle. It can be also observed that when the traffic load is light relative to a certain combination, energy consumption increases approximately linearly with packet generating interval. For example, the traffic load is relatively light at the top three points under the combination of (1,0), which can be proved at the corresponding points with very low PLR values on the PLR graph as shown in Figure 4(b).

Another trend revealed by each single curve on the energy graph is that under the same traffic load, the network needs more energy to transmit one payload byte when configured with a larger combination of BO and SO. This is especially obvious for the mean message interval of 0.01 s curve, which is the highest one among all the traffic loads. In fact for the same traffic load, the relative traffic condition becomes heavier as the length of BI increases while the duty cycle keeps constant. This can be proved by the increasing PLR as shown in the PLR graph in Figure 4(b). Since the packet interval is the same for one curve, the higher PLR means that less packets have been received per time unit, which is clearly shown in the goodput graph in Figure 4(d). However, the mean energy consumption per time unit will remain approximately the same independent of the values of BO and SO, because the node is always busy sending or receiving packets while the PLR is not low and the duty cycle dominates the overall energy consumption. Therefore, it can be concluded from the above analysis that when averaged to each transmitted payload byte, the mean energy consumption will increase with the values of BO and SO.

Figure 4(b) shows the measured end-to-end PLR, which reveals the capacity of the network under various parameter settings. For the same (BO,SO), the PLR increases with the traffic load, which is self-explaining. The reason for each curve ascending as the BI becomes longer is due to the increasing relative traffic load, which has been explained previously. Comparing all the curves in the graph, we can notice that the PLR curve rises earlier under higher packet generating rate, which is the combination result of the previous two rules. It can be observed from the PLR graph that the (1,0) combination has the largest capacity.

Figure 4(c) depicts the measured mean end-to-end delay on a logarithmic scale. For the small (BO,SO) as shown on the left-hand side of the graph, the delay stays at a very low level, independent of the applied traffic load. The reason is that all the traffic conditions are relatively light at the small (BO,SO) values. Most packets can be transmitted successfully

DOI: 10.1002/wcm

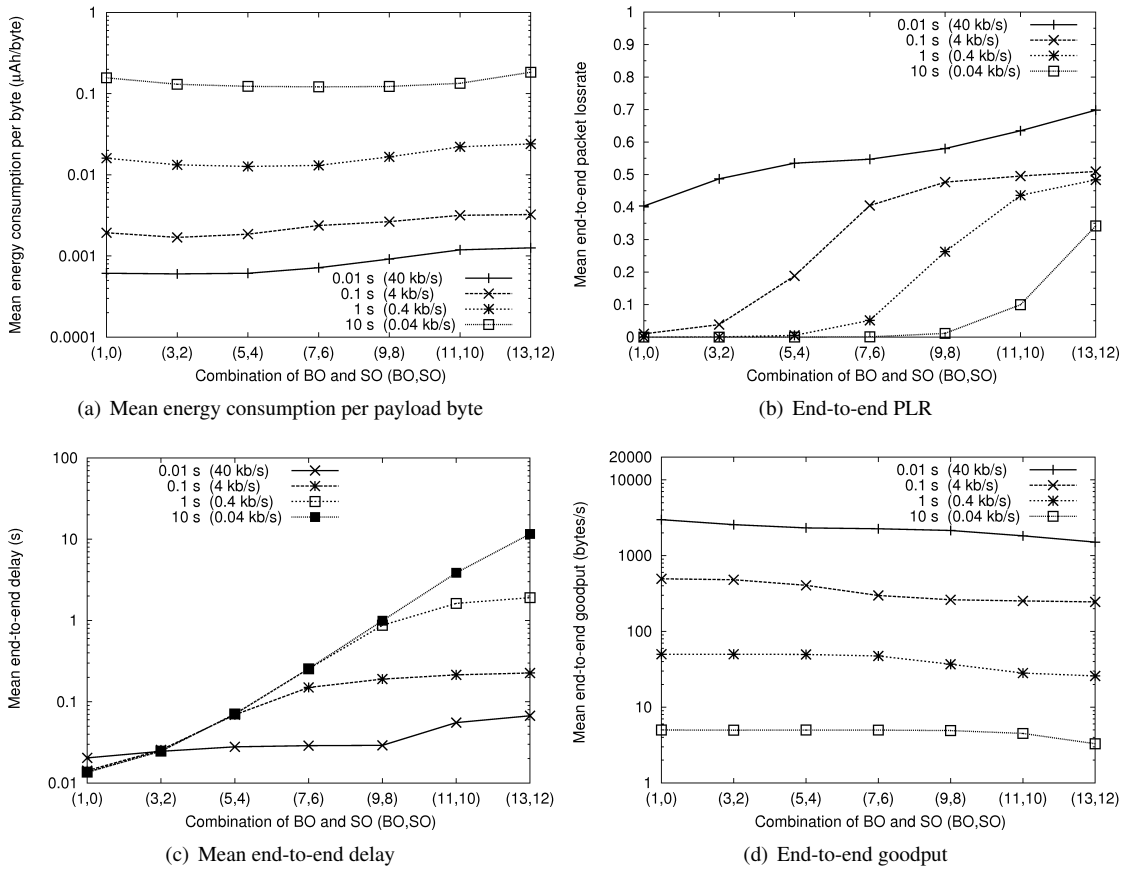

(a) Mean energy consumption per payload byte

(b) End-to-end PLR

(c) Mean end-to-end delay

(d) End-to-end goodput

Fig. 4. CSMA/CA: energy and end-to-end performance for different combination of BO and SO with 50% duty cycle under various traffic loads

from the source to the sink with a high delivery rate and very few packets suffer from long waiting time in the queue due to contending for the channel or going through the sleeping period. We can notice that at (1,0), the delay under the load of 0.01 s is a little higher than that under the other traffic conditions. This can be explained by the higher loss rate as shown in the PLR graph due to the higher traffic load. In this case more packets have to wait in the queue for the next active period at the intermediate node before they can be forwarded to the sink. Since the sleeping period is only about 15 ms when SO=0, the extra queue delay will not significantly increase the overall mean delay. When the the values of (BO,SO) increase, the delay curve ascends because of the increased inactive period, which introduces longer queue delay.

Another interesting phenomenon in the delay measurements can be observed for the (BO,SO) combination of (13,12) on the right-hand side of the graph. The mean delay for the packet interval of 10 s is about 10 s, which is three orders of magnitude bigger than the mean delay for the packet interval of 0.01 s. Such huge difference is mainly caused by the long BI and SD, which equal to 126 s and 63 s, respectively, for the (BO,SO) combination of (13,12). Because the length of active period is much longer than the packet interval in all the traffic conditions, the number of transmitted packets per BI will increase approximately linearly with the number of packets generated per BI, which can be proved by the goodput graph shown in Figure 4(d). Within a beacon interval, since the IFQ size is set to 1, at most two packets (one in the IFQ and one at MAC) will suffer from a fairly long delay due to the long inactive period of 63 s at (13,12). In general, the overall mean end-to-end delay in this case is determined to a certain extent by the number of those packets, which are sent immediately within a beacon interval without experiencing a long inactive period. Therefore, the much smaller delay at the higher traffic load is contributed by the large amount of

DOI: 10.1002/wcm

small delays per BI that have largely averaged a few extremely large delays to a small value.

Figure 4(d) shows the measured end-to-end goodput on a logarithmic scale. Compared with those in the energy graph as shown in Figure 4(a), the curves for goodput show a similar but inverse trend. Under the same duty cycle, the goodput is mainly determined by the traffic load and shows less dependency on the other parameters. According to the queuing, when the traffic is very light and no packets get lost in the network, the number of packets outgoing per time unit should be equal to the number of packets arriving per time unit. In the goodput graph, this theory applies at those points that are corresponding to about zero loss in the PLR graph, which partially validates our simulation results. Under the same traffic load, the goodput decreases with the increase of the (BO,SO) due to the rising PLR, which has been explained previously.

4.1.2. Scenario 2: 21 nodes, effects of BO and SO

In the previous section, we investigated the performance of a three-node star network by exploring various (BO,SO) combinations of 50% duty cycle, which is regarded as a starting point of our study. Now, we simulate a larger star network, which models a typical application using WSN techniques in industrial control fields. The scenario can be described as follows: 20 devices equipped with various sensors are scattered within an area and associated to a central node, the PAN coordinator, to form a monitoring or control network. Upon detecting that single readings exceed a predefined threshold, a short alarm message with only one Byte payload must be sent to the PAN coordinator within a well-specified time. For such applications, low-latency is usually put in the first place, while energy efficiency is also another important consideration. Since one of these two aspects is usually achieved by sacrificing the other on performance, simuations can help us to find out a proper balance point for a certain requirement.

The topology of this scenario has been shown previously in Figure 3. 20 devices are placed symmetrically around the PAN coordinator with an equal distance of 30 meters to each of their neighbors. Communications only occur between the devices and the PAN coordinator. Each device sends packets generated by its own exponential traffic source to the PAN coordinator. The packet generating interval is varied between 0.01 s and 100 s. Due to large range of the packet interval, logarithmic scaling has been used on the horizontal axis on all the graphs. For similar reasons, logarithmic scaling has been also applied on the vertical axis on all the graphs except for that for PLR.

Fixed SO and various BO – In the first set of experiments, we fixed SO to 0, which results in a constant active period of $0.015\,\mathrm{s}$. The BO is chosen at 1, 3, 5, and 7, which correspond to the beacon interval of $0.03\,\mathrm{s}$, $0.12\,\mathrm{s}$, $0.49\,\mathrm{s}$, and $1.97\,\mathrm{s}$, respectively. We also varied the mean packet inter arrival time between $0.01\,\mathrm{s}$ and $100\,\mathrm{s}$. Figure 5(a) shows the measured mean end-to-end PLR. Similar to the first scenario, packet loss occurs either due to IFQ overflow or due to exceeding the maximum number of retransmissions caused by collisions. With decreasing traffic load, the PLR descends from the top value of near 100% gradually down to a small value close to zero. The curve with a smaller BO starts to decline earlier, showing the stronger capacity due to its higher duty cycle. Because we configured the IFQ to 1, as long as the queue is full, i.e. for higher traffic rates, collisions will exist. Thus, the PLR is caused by two effects: tail drop at the IFQ (dominating at higher traffic rates) and collisions in the MAC (dominating at lower traffic rates).

The measured mean energy consumption per payload byte is depicted in Figure 5(b). In the area of heavy traffic load on the left-hand side of the graph, the energy consumption under the same traffic load increases with the increasing length of BI. For example for a traffic interval of 0.01 s, due to the same length of the active period, the average number of packets transmitted per BI are almost the same for various SO. This means that almost the same amount of energy is consumed in the active period. Therefore, the longer BI consuming more energy is caused by more energy consumption in the inactive period. Under heavy traffic, the energy consumption on each curve remains constant independent of the traffic load, because the MAC is almost fully loaded. The total energy consumed in the active period has reached its peak value and the number of transmitted packets per BI is saturated, which can be seen in the goodput graph. Therefore, the total energy averaged to each payload byte is constant. As the traffic load keeps decreasing, the energy curve drops first and then ascends monotonously. The drop in energy consumption is contributed by the decrease in the number of collisions per BI, which reduces the energy wasted in resending. The starting point for descending

DOI: 10.1002/wcm

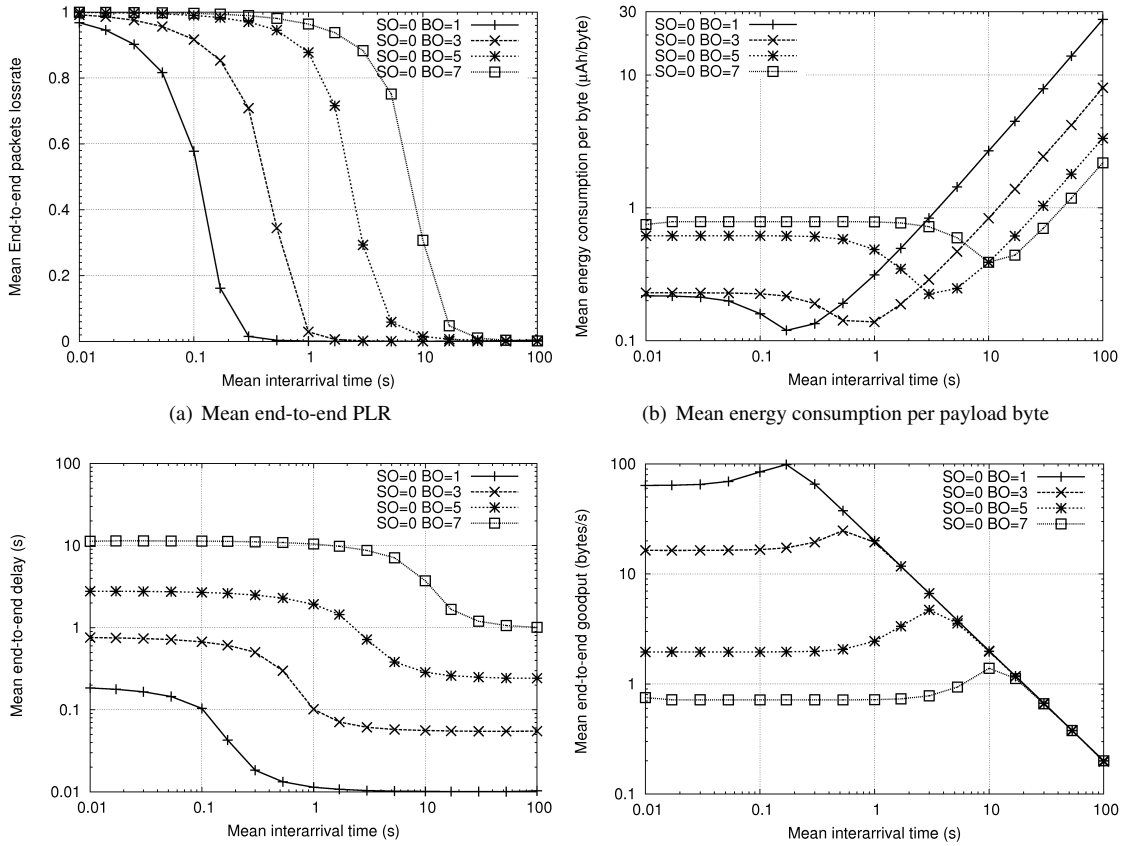

(a) Mean end-to-end PLR

(b) Mean energy consumption per payload byte

(c) Mean end-to-end delay

(d) Mean end-to-end goodput

Fig. 5. CSMA/CA: energy and end-to-end performance for SO=0 and various values of BO under various traffic loads

on the energy graph is right the turning point at which the PLR at the IFQ has dropped to a low level and the PLR at the MAC starting to decrease, as mentioned previously. When the collision rate has bottomed out, the energy consumption reaches its minimum value at this point. The increasing trend in energy consumption on the right-hand side of the graph can be explained as follows. As the traffic load gets lighter, less packets are transmitted per BI and the ratio of energy consumed on idle listening increases. When idle listening starts to contribute to the most percentage of the overall energy consumption, the mean energy consumption per payload byte will increase inverse proportionally to the packet generating rate. In the area of energy ascending on all the curves, the smallest BO consumes the most energy, because with the same SO higher duty cycle under light traffic means more energy consumption per unit time. However, the number of packets transmitted per time unit are almost the same, which can also be explained on the goodput graph as shown in Figure 5(d).

Figure 5(c) shows the measured mean end-to-end delay on a logarithmic scale. At the same packet interval, the smaller BO with the same SO achieves lower latency benefiting from its shorter inactive period, in which the buffered packets may experience a relatively long delay. In the case of very light traffic load, the end-to-end delay remains at its theoretic minimum value, which is contributed mainly by random backoff delay, transmission delay and sleeping delay and suffers little from delays in queuing, additional backoffs or retransmission. As the traffic load increases, the end-to-end delay rises due to the increasingly intense contention on the channel and the rising number of collisions. However, as the traffic load gets heavier and heavier, the delay will not keep rising but stay at a saturation value, because the MAC reaches its maximum ability and most packets are dropped at the IFQ.

Figure 5(d) shows the measured mean end-to-end

DOI: 10.1002/wcm

goodput. Under high traffic load, the smaller BO resulting in higher duty cycle can achieve much better bandwidth utilization and, therefore, much higher goodput. As the traffic load goes lighter, the goodput will reach its peak value at the same point on the traffic load axis as on the energy graph, where the minimum energy consumption per byte is achieved because the collision rate has reached minimum while the channel is still fully utilized at a critical point. As the traffic load keeps decreasing, the goodput curve goes down monotonously, the level of which is determined by the packet generating rate. When the traffic load is low enough, for example at the interval of 100 seconds, the goodput becomes parameter-independent within a certain variation range of BO, because the packet interval is much longer than the BI in all the cases and the goodput is basically the same with the packet inter-arrival rate.

Fixed BO and various SO – In the second set of experiments, we consider a constant beacon interval by fixing BO to 8 and study the effect of various active period by choosing SO at 0, 2, 4 and 6. The modification of SO leads to different duty cycle, which dominates the overall performance. The simulation results are depicted in Figure 6. In all figures, the obtained results for different SO under the same traffic load underline the effects described for the previous measurement (fixed SO) and reproduce the same trend. Under heavy traffic loads, SO with larger value resulting in a higher duty cycle achieves better energy and end-to-end performance. As the traffic gets lighter, such advantage in end-to-end performance remains but follows a weakening trend, especially in end-to-end delay and goodput as shown in Figure 6(c) and in Figure 6(d). However, when the traffic load is light, lower duty cycle shows more advantage in energy-saving, which can be observed on the right hand side of Figure 6(b).

Finally, the end-to-end delay curves in Figure 6(c) need to be discussed. It is common to see as appeared at the higher two curves that the delay increases as the traffic gets heavier, due to more collisions. However, the lower two curves with larger SO values show an opposite trend. This effect has been explained previously when we analyzed the similar phenomenon that appears in Figure 4(c). Longer active period with larger SO has more ability to transmit packets within current superframe without making them suffer from sleeping period. Since we set the IFQ size to only 1, at most two packets will experience long sleeping delay. The decreasing mean delay at large SO with the increasing traffic load is mainly caused by the fact that more and more small delays are averaging a relatively constant number of long delays to a smaller value.

To sum up the above performance analysis, each curve in the graphs shown in Figures 5 and 6 can be divided into three areas according to the degree of the relative traffic load, which include the areas for heavy traffic, moderate traffic, and light traffic. In the heavy traffic area, the higher duty cycle under the same SO can achieve better performance in both the energy consumption and the end-to-end aspects. This rule will still apply when the traffic load decreases from high to moderate. Under very light traffic, which is usually the case in most sensor network applications, especially in our studied scenario aiming at industrial applications, higher duty cycle achieves lower latency at the cost of more energy consumption. Such a trade-off between energy efficiency and low-latency can be optimized through carefully choosing the combination of the parameters BO and SO, which dominate the overall performance, according to the requirements by the specific applications. Our performance study based on a typical industrial application has revealed the complex relation among energy consumption, end-to-end performance, parameter configurations and traffic loads. The simulation results can support such optimization problems.

4.2. Second Experiment: IEEE 802.15.4 GTS

In our second experiment, we evaluate the GTS scheme that the IEEE 802.15.4 has proposed to provide guaranteed service for real-time applications. Considering the deterministic and independent characteristics of TDMA-like scheme, we investigate only one GTS allocation in a star network with only one device and one PAN coordinator. According to our implementation, a device desiring for GTS can directly requests one GTS from the PAN coordinator at the starting stage of the simulation running. In our current IEEE 802.15.4 GTS model, neither allocation nor deallocation process exactly defined in the specification is modeled. In this experiment, the length of the GTS is allocated with a minimal number of superframe slots, which can accommodate at least one complete transaction for transmitting one alarm message with only one Byte payload. Since no collision will occur within the GTS, the GTS model is configured to run in the none-acknowledgment mode. Using the same (BO,SO) combinations as in Figure 5, we fixed SO to 0 and explored various BO at 1, 3, 5 and 7. The obtained results are shown in Figure 7.

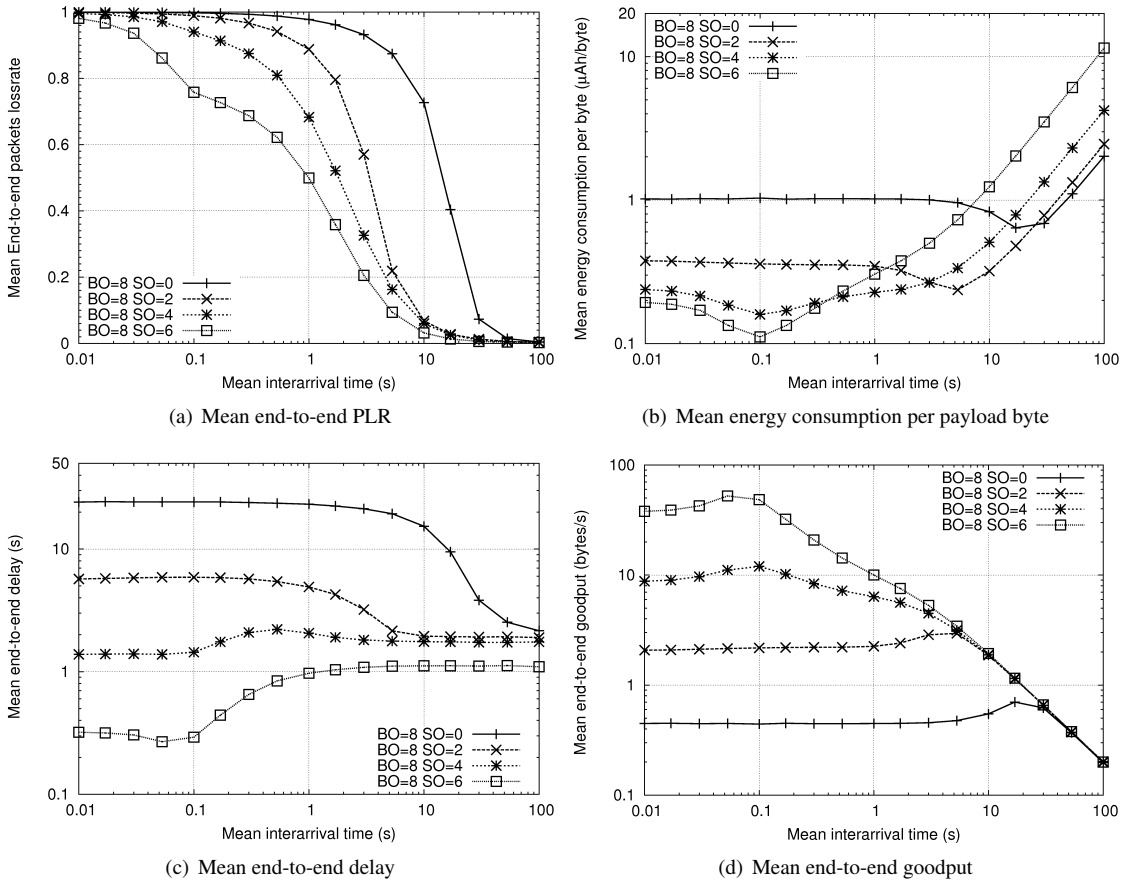

(a) Mean end-to-end PLR

(b) Mean energy consumption per payload byte

(c) Mean end-to-end delay

(d) Mean end-to-end goodput

Fig. 6. CSMA/CA: energy and end-to-end performance for BO=8 and various values of SO under various traffic loads

Figure 7(a) shows the measured PLR. The curves with larger BO are higher because of the longer inactive period. Since no collision exists in GTS, packets get loss only at the IFQ due to buffer overflow. This can be also used to explain why the goodput curves that are shown in Figure 7(d) do not generate a wave crest, which has been observed in previous experiment for CSMA/CA. Under heavy traffic load, higher duty cycle achieves higher maximum goodput. Normally for combined TDMA-based and schedule-based MAC protocol, the maximum goodput is mainly determined by the allocated bandwidth and the duty cycle. In this experiment, the bandwidth allocated for the GTS for various BO is same due to the same SO and constant payload in messages. Therefore, the various BO that determines the duty cycle, has a major effect on the maximum goodput. Theoretically, it is easy to estimate that if the beacon interval is doubled (BO increased by 1), the maximum goodput should be halved. This estimation can be validated by the results in Figure 7(d). For example, the maximum goodput at about $103.2\,\mathrm{bytes/s}$ for BO equal to 1 is approximately four times larger than the one for BO equal to 3, which is at about $32.6\,\mathrm{bytes/s}$.

The measured energy consumption is shown in Figure 7(b). The energy curves for GTS follow the similar trend that is shown in Figure 5(b) without producing a wave trough, because no retransmission in the collision-free GTS will occur and consume energy. Figure 7(c) shows the measured mean end-to-end delay, which follows a regular trend as expected. The saturated value at each curve on the left part of the figure represents the maximum delay that the GTS can guarantee for a certain (BO,SO) combination. These maximum delays obtained from the simulations can be easily validated through worst case analysis. Independent of the number of GTSs per superframe, the worst case happens when a message is generated at a device during its own GTS slot. At this time, the device cannot transmit the message immediately

DOI: 10.1002/wcm

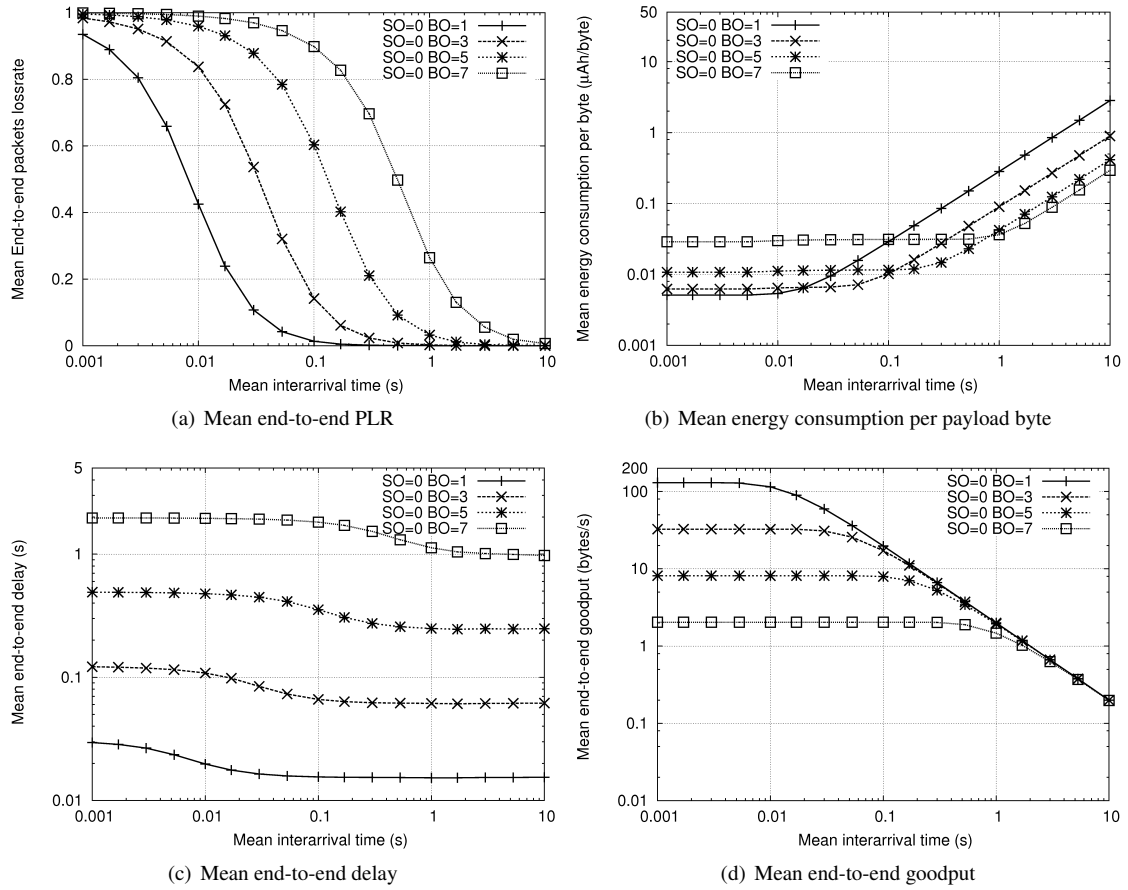

(a) Mean end-to-end PLR

(b) Mean energy consumption per payload byte

(c) Mean end-to-end delay

(d) Mean end-to-end goodput

Fig. 7. GTS: energy and end-to-end performance for SO=0 and various values of BO under various traffic loads

and must buffer the message. The buffered message must wait for one beacon interval until the start of the corresponding GTS in the next superframe and needs a transaction period to get transmitted. Therefore, the guaranteed maximum delay under the worst case is bounded by the sum of one beacon interval and one transaction duration. We take BO equal to 5 for example. The resulting beacon interval is $0.49\,\mathrm{s}$. According to the specification, the duration for transmitting one message with one Byte payload requires less than $1\,\mathrm{ms}$, which can be ignored compared to the beacon interval. Therefore, the theoretically estimated value for the guaranteed maximum delay is around the value of a beacon interval. As we can see in Figure 7(c), the saturation area on the curve for BO equal to 5, which is at around $0.5\,\mathrm{s}$, is very close to this estimated value.

5. Conclusion and Future Work

We presented and intensively discussed a number of performance measures of the IEEE 802.15.4 protocol. In essence, we obtained these results in a simulative performance study on our IEEE 802.15.4 simulation model that has been implemented for OMNeT++. We analyzed two different scenarios for the CSMA/CA operation mode: one with a small three-node star topology and the other with a 21-nodes star network modeling a typical industrial sensor network application. In addition, we analyzed the GTB mode that allows real-time operation based on a TDMA schedule. The simulation results for one energy measure and three end-to-end measures were analyzed in detail, which can be used to support the parameter configuration and optimization in IEEE 802.15.4 based sensor networks.

In future work, we will continue to study the applicability of IEEE 802.15.4 in low-latency and energy-aware applications especially in industrial

control fields. Based on our findings, we are working on improved versions of the protocol for application in various scenarios focusing on low-energy consumption with strict quality of service constraints such as delay bounds. This work is also supported by recent findings of other groups in the context of improved real-time operation. In conclusion, it can be said that there is still room for improvements, e.g. using slotted CSMA/CA for time-critical events [10], priority-based delay mitigation [9], and special GTS allocation mechanisms for time sensitive networks [12].

Furthermore, we only investigated simple models of the physical radio channel. It is necessary to continue our work by implementing more sophisticated channel models that also incorporate random fluctuations that will typically appear in industrial automation scenarios.

References

1. I. F. Akyildiz, W. Su, Y. Sankarasubramaniam, and E. Cayirci. Wireless sensor networks: a survey. *Elsevier Computer Networks*, 38:393–422, 2002.
2. P. Baronti, P. Pillai, V. W. Chook, S. Chessa, A. Gotta, and Y. F. Hu. Wireless Sensor Networks: a Survey on the State of the Art and the 802.15.4 and ZigBee Standards. *Elsevier Computer Communications*, 30(7):1655–1695, May 2007.
3. B. Bougard, F. Catthoor, D. C. Daly, A. Chandrakasan, and W. Dehaene. Energy Efficiency of the IEEE 802.15.4 Standard in Dense Wireless Microsensor Networks: Modeling and Improvement Perspectives. In *8th IEEE/ACM Conference on Design, Automation, and Test in Europe (DATE 2005)*, pages 196–201, Munich, Germany, March 2005. IEEE.
4. F. Chen and F. Dressler. A Simulation Model of IEEE 802.15.4 in OMNeT++. 6. GI/ITG KuVS Fachgespräch Drahtlose Sensornetze, Poster Session, July 2007.
5. F. Chen, N. Wang, R. German, and F. Dressler. Performance Evaluation of IEEE 802.15.4 LR-WPAN for Industrial Applications. In *5th IEEE/IFIP Conference on Wireless On demand Network Systems and Services (IEEE/IFIP WONS 2008)*, pages 89–96, Garmisch-Partenkirchen, Germany, January 2008. IEEE.
6. A. Cunha, A. Koubaa, R. Severino, and M. Alves. Open-ZB: an open-source implementation of the IEEE 802.15.4/ZigBee protocol stack on TinyOS. In *4th IEEE International Conference on Mobile Ad Hoc and Sensor Systems (IEEE MASS 2007)*, pages 1–12, October 2007.
7. IEEE. Wireless Medium Access Control (MAC) and Physical Layer (PHY) Specifications for Low Rate Wireless Personal Area Networks (WPANs). IEEE Sandard 802.15.4-2006, 2006.
8. P. Jurcik, A. Koubaa, M. Alves, E. Tovar, and Z. Hanzalek. A Simulation Model for the IEEE 802.15.4 Protocol: Delay/Throughput Evaluation of the GTS Mechanism. In *15th IEEE International Symposium on Modeling, Analysis, and Simulation of Computer and Telecommunication Systems (MASCOTS 2007)*, pages 109–116, Istanbul, Turkey, October 2007.
9. T. H. Kim and S. Choi. Priority-Based Delay Mitigation for Event-Monitoring IEEE 802.15.4 LR-WPANs. *IEEE Communications Letters*, 10(3):213–215, March 2006.
10. A. Koubaa, M. Alves, B. Nefzi, and Y.-Q. Song. Improving the IEEE 802.15.4 Slotted CSMA/CA MAC for Time-Critical Events in Wireless Sensor Networks. In *5th International Workshop on Real-Time Networks (RTN 2006)*, Dresden, Germany, July 2006.
11. A. Koubaa, M. Alves, and E. Tovar. A comprehensive simulation study of slotted CSMA/CA for IEEE 802.15.4 wireless sensor networks. In *5th IEEE International Workshop on Factory Communication Systems (WFCS 2006)*, pages 183–192, Torino, Italy, 2006.
12. A. Koubaa, M. Alves, and E. Tovar. i-GAME: An Implicit GTS Allocation Mechanism in IEEE 802.15.4 for Time-Sensitive Wireless Sensor Networks. In *18th Euromicro Conference on Real-Time Systems (ECRTS 2006)*, pages 183–192. IEEE, July 2006.
13. O. Landsiedel, K. Wehrle, and S. Götz. Accurate Prediction of Power Consumption in Sensor Networks. In *Second IEEE Workshop on Embedded Networked Sensors (EmNetS-II)*, Sydney, Australia, May 2005.
14. V. B. Misic, J. Fung, and J. Misic. MAC Layer Security of 802.15.4-Compliant Networks. In *2nd IEEE International Conference on Mobile Ad Hoc and Sensor Systems (IEEE MASS 2005): 1st IEEE International Workshop on Wireless and Sensor Networks Security (IEEE WSNS 2005)*, Washington, DC, November 2005.
15. A. Varga. The OMNeT++ Discrete Event Simulation System. In *European Simulation Multiconference (ESM 2001)*, Prague, Czech Republic, June 2001.
16. W. Ye, J. Heidemann, and D. Estrin. An Energy-Efficient MAC Protocol for Wireless Sensor Networks. In *21st IEEE Conference on Computer Communications (IEEE INFOCOM 2002)*, volume 3, pages 1567–1576, New York, NY, June 2002.
17. J. Zheng and M. J. Lee. A Comprehensive Performance Study of IEEE 802.15.4. In *Sensor Network Operations*, pages 218–237. IEEE, 2006.
18. Zigbee Alliance. Zigbee Specification. Technical report, 2006.

DOI: 10.1002/wcm